

1 *Supplement of*

2 **Large contribution of soil emissions to the atmospheric nitrogen**

3 **budget and their impacts on air quality and temperature rise in**

4 **North China**

5 *Tong Sha¹*, Siyu Yang¹, Qingcai Chen¹, Liangqing Li¹, Xiaoyan Ma², Yan-Lin Zhang^{3,4},*

6 *Zhaozhong Feng³, K. Folkert Boersma^{5,6}, Jun Wang^{7*}*

7 ¹School of Environmental Science and Engineering, Shaanxi University of Science and
8 Technology, Xi'an 710021, China

9 ² Key Laboratory for Aerosol-Cloud-Precipitation of China Meteorological
10 Administration, Nanjing University of Information Science & Technology, Nanjing
11 210044, China

12 ³ School of Ecology and Applied Meteorology, Nanjing University of Information
13 Science & Technology, Nanjing 210044, China

14 ⁴ Atmospheric Environment Center, Joint Laboratory for International Cooperation on
15 Climate and Environmental Change, Ministry of Education (ILCEC), Nanjing
16 University of Information Science & Technology, Nanjing 210044, China

17 ⁵ Satellite Observations Department, Royal Netherlands Meteorological Institute, De
18 Bilt 3731GA, the Netherlands

19 ⁶ Meteorology and Air Quality Group, Wageningen University Wageningen 6708PB,
20 the Netherlands

21 ⁷ Department of Chemical and Biochemical Engineering, Center for Global and
22 Regional Environmental Research, and Iowa Technology Institute, University of Iowa,
23 Iowa City, IA, 52242, USA

24 *Corresponding authors:

25 Tong Sha: tong-sha@sust.edu.cn

26 Jun Wang, jun-wang-1@uiowa.edu

27

28 **Text S1. Parameterization of HONO sources**

29 In the present study, we incorporated five additional HONO sources in the WRF-
 30 Chem model, as described below.

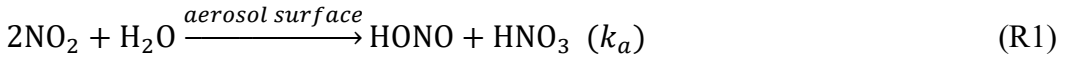
31 1. Direct traffic emissions

32 The traffic emission was calculated by a HONO/NO_x ratio of 1.7% (Rappenglück
 33 et al., 2013), which is the same as the setting of (Zhang et al., 2019).

34 2. The HONO source from soil emissions

35 See section 2.1.2 in the manuscript.

36 3. Heterogeneous source on aerosol surface



38 Most studies suggested that the heterogeneous reaction of NO₂ to HONO was first
 39 order in NO₂ (Finlayson-Pitts et al., 2003; Saliba et al., 2000), thus for the NO₂
 40 heterogeneous reaction on the aerosol surface, the first-order reaction rate constant k_a
 41 is estimated by (Li et al., 2010) and (Zhang et al., 2016) as follows:

42 $k_a = \frac{1}{4} \cdot v_{\text{NO}_2} \cdot \left(\frac{S_a}{V}\right) \cdot \gamma_{\text{a-NO}_2}$ (1)

43 where v_{NO_2} is the mean molecular velocity of NO₂ (m s⁻¹), S_a/V is the aerosol surface
 44 to volume ratio (m⁻¹) representing the surface available for heterogeneous reaction.
 45 $\gamma_{\text{a-NO}_2}$ is the uptake coefficient of NO₂ at the aerosol surface, which was set to be $1 \times$
 46 10^{-6} for nighttime, and a higher value of 2×10^{-5} applied for daytime when the light
 47 intensity (LI) was lower than 400 W m⁻², whereas we linearly scaled it with solar
 48 radiation when the light intensity was higher than 400 W m⁻² (equation 2).

49
$$\gamma_{\text{a-NO}_2} = \begin{cases} 1 \times 10^{-6} & (\text{nighttime}) \\ 2 \times 10^{-5} \cdot \left(\frac{\text{LI}}{400}\right) & (\text{daytime}, \text{LI} \geq 400 \text{W m}^{-2}) \\ 2 \times 10^{-5} & (\text{daytime}, \text{LI} < 400 \text{W m}^{-2}) \end{cases}$$
 (2)

50 4. Heterogeneous source on ground surface



52 For the NO₂ heterogeneous reaction on ground surface (R2), the first-order
 53 reaction rate constant k_g is estimated by (Zhang et al., 2016) as follows:

54 $k_g = \frac{1}{8} \cdot v_{\text{NO}_2} \cdot \left(\frac{S_g}{V}\right) \cdot \gamma_{\text{g-NO}_2}$ (3)

55 where v_{NO_2} is the mean molecular velocity of NO_2 (m s^{-1}), S_g/V represents the ground
56 surface to volume ratio. Over the urban areas as defined by the MODIS land use data,
57 we adopted a constant S_g/V value of 0.3 m^{-1} . For the vegetation-covered areas, the leaf
58 area index (LAI, m^2/m^2) and the height of the first model layer (H , m) were used to
59 estimate the surface area to volume ratio following the method in (Sarwar et al., 2008):

60
$$\frac{S_g}{V} = \frac{2 \times \text{LAI}}{H} \quad (4)$$

61 $\gamma_{g-\text{NO}_2}$ is the uptake coefficient of NO_2 at the ground surface and is assumed to be the
62 same as that for aerosol surface. The heterogeneous reaction of NO_2 on the ground
63 surface was only considered within the first model layer, whereas that on the aerosol
64 surface was treated in all model layers.

65 5. Inorganic nitrate photolysis

66 The photolysis reaction of particulate nitrate in the atmosphere to produce HONO
67 and NO_2 (R3) was added in the WRF-Chem model following the work of (Fu et al.,
68 2019).



70 The photolysis rate of particulate nitrate was estimated by a $J_{\text{nitrate}}/J_{\text{HNO}_3}$ ratio of
71 $\frac{8.3 \times 10^{-5}}{7 \times 10^{-7}}$, where J_{HNO_3} is the photolysis rate of gaseous HNO_3 simulated online in the
72 model.

73

74 **Table S1** Total annual N fertilizer application from 2006 to 2018 (unit: 10 Gg N yr⁻¹),
 75 and the adjustment coefficient (2006 vs. 2018, unit: %) for N fertilizer application in
 76 each province.

| Province | 2006 | 2007 | 2008 | 2009 | 2010 | 2011 | 2012 | 2013 | 2014 | 2015 | 2016 | 2017 | 2018 | 2006vs.2018 |
|------------------|------|------|------|------|------|------|------|------|------|------|------|------|------|-------------|
| Neimenggu | 64 | 68 | 73 | 80 | 80 | 81 | 83 | 89 | 97 | 99 | 98 | 95 | 86 | 34.5 |
| Gansu | 37 | 38 | 38 | 38 | 38 | 38 | 40 | 40 | 41 | 41 | 39 | 34 | 33 | -9.6 |
| Ningxia | 16 | 17 | 17 | 17 | 18 | 18 | 18 | 19 | 18 | 17 | 17 | 17 | 16 | 4.5 |
| Shaanxi | 76 | 81 | 81 | 87 | 88 | 91 | 98 | 99 | 96 | 94 | 92 | 90 | 89 | 16.2 |
| Shanxi | 41 | 41 | 40 | 39 | 40 | 39 | 39 | 38 | 36 | 34 | 32 | 28 | 25 | -38 |
| Hebei | 155 | 156 | 153 | 153 | 153 | 152 | 152 | 151 | 151 | 148 | 145 | 140 | 114 | -26.2 |
| Beijing | 8 | 7 | 7 | 7 | 7 | 7 | 6 | 6 | 5 | 5 | 4 | 4 | 3 | -61.3 |
| Tianjin | 12 | 13 | 12 | 12 | 12 | 11 | 11 | 11 | 11 | 10 | 9 | 7 | 6 | -53.6 |
| Henan | 235 | 239 | 240 | 239 | 244 | 245 | 246 | 244 | 241 | 239 | 228 | 220 | 202 | -14.3 |
| Shandong | 194 | 193 | 170 | 165 | 163 | 159 | 160 | 158 | 154 | 151 | 146 | 139 | 131 | -32.5 |
| Jiangsu | 183 | 183 | 181 | 182 | 180 | 174 | 169 | 166 | 164 | 162 | 158 | 151 | 146 | -20.4 |
| Anhui | 112 | 111 | 112 | 112 | 112 | 114 | 114 | 114 | 112 | 108 | 105 | 101 | 96 | -14.4 |
| Hubei | 140 | 143 | 149 | 154 | 156 | 159 | 159 | 153 | 146 | 139 | 134 | 128 | 113 | -19.5 |
| Chongqing | 46 | 48 | 50 | 50 | 49 | 50 | 50 | 50 | 50 | 50 | 48 | 47 | 46 | -1.1 |
| Sichuan | 125 | 128 | 129 | 131 | 130 | 129 | 128 | 126 | 126 | 125 | 122 | 117 | 112 | -10.1 |
| Liaoning | 63 | 65 | 66 | 67 | 68 | 70 | 68 | 70 | 68 | 66 | 60 | 57 | 55 | -13.5 |

77

78 **Table S2.** Soil categories used in (Oswald et al., 2013).

| No. | Soil Category in Oswald et al. (2013) |
|------------|--|
| S1 | eucalyptus forest, Grose Valley, Australia |
| S2 | tropical rain forest, Suriname |
| S3 | coniferous forest, Hohenpeißenberg, Germany |
| S4 | coniferous forest, Fichtelgebirge, Germany |
| S5 | pasture, Hawkesbury River flood plain, Australia |
| S6 | open woody savannah, Dahra, Senegal |
| S7 | open woody savannah, Agoufou, Mali |
| S8 | grassland, Mainz-Finthen, Germany |
| S9 | pasture, Hohenpeißenberg, Germany |
| S10 | stone desert, Ruta B 376, Chile |
| S11 | maize field, Grignon, France |
| S12 | wheat field, Mainz-Finthen, Germany |
| S13 | jujube field, Qiemo, China |
| S14 | cotton field, Qiemo, China |
| S15 | jujube field, Mingfeng, China |
| S16 | stone desert, Sache, China |
| S17 | cotton field, Milan, China |

Table S3. Emission factor of 20 soil biomes based on MODIS land cover types.

| ID | MODIS land cover type | MEDIUM | HIGH | LOW |
|----|------------------------------------|--------------------------------|------|-----|
| 1 | Evergreen needleleaf forest | S3, S4 | S3 | S4 |
| 2 | Evergreen broadleaf forest | S2 | S2 | S2 |
| 3 | Deciduous needleleaf forest | S3, S4 | S3 | S4 |
| 4 | Deciduous broadleaf forest | S1 | S1 | S1 |
| 5 | Mixed forest | S1, S2, S3, S4 | S2 | S4 |
| 6 | Closed shrublands | S6, S7, S8 | S6 | S8 |
| 7 | Open shrublands | S6, S7 | S6 | S7 |
| 8 | Woody savannas | -- | -- | -- |
| 9 | Savannas | S6, S7 | S6 | S7 |
| 10 | Grasslands | S8 | S8 | S8 |
| 11 | Permanent wetlands | -- | -- | -- |
| 12 | Croplands | S5, S9, S11, S12, S14, S17 | S12 | S9 |
| 13 | Urban and built-up | -- | -- | -- |
| 14 | Cropland/Natural vegetation mosaic | S8, S5, S9, S11, S12, S14, S17 | S12 | S9 |
| 15 | Snow and ice | -- | -- | -- |
| 16 | Barren or sparsely vegetated | S16, S10 | S10 | S16 |
| 17 | water | -- | -- | -- |
| 18 | Wooded tundra | -- | -- | -- |
| 19 | Mixed tundra | -- | -- | -- |
| 20 | Barren Tundra | -- | -- | -- |

Table S4. The optimum SHONO fluxes used in this study and other literature.

| ID | MODIS land cover type | Optimum SHONO fluxes (ng m ⁻² s ⁻¹) | References (land cover type in local scale) |
|----|------------------------------------|---|--|
| 1 | Evergreen needleleaf forest | 0.549 | this study |
| 2 | Evergreen broadleaf forest | 2.872 | this study |
| 3 | Deciduous needleleaf forest | 0.549 | this study |
| 4 | Deciduous broadleaf forest | 0.887 | this study |
| | | 1.214 | this study |
| | | 1.3 | Zhou et al. (2011) |
| 5 | Mixed forest | 0.01-104.72 (mean=16.45) | Wu et al. (2022) |
| | | 0.2-208 (mean=50) | Wang et al. (2023) |
| 6 | Closed shrublands | 20.57 | this study |
| 7 | Open shrublands | 29.779 | this study |
| 8 | Woody savannas | -- | -- |
| | | 9.926 | this study |
| 9 | Savannas | 1.1 | Weber B (2015) |
| | | 2.154 | this study |
| 10 | Grasslands | 1.0 | Twig et al. (2011) |
| | | 0.1-74.27(mean =17.57) | Wu et al. (2022) |
| 11 | Permanent wetlands | -- | -- |
| | | 30.036 | this study |
| | | 1.42-376.01(mean =119.8) | Wu et al. (2019, 2022) |
| 12 | Croplands | 0.84±2.38 | Meng et al. (2022) |
| | | -1.32-7.69 (mean=2.94) | Tang et al. (2020) |
| | | 3.21 | Xue et al. (2019) |
| | | 16-484 | Wang et al. (2023) |
| 13 | Urban and built-up | -- | -- |
| 14 | Cropland/Natural vegetation mosaic | 25.847 | this study |
| 15 | Snow and ice | -- | -- |
| 16 | Barren or sparsely vegetated | 14.742 | this study |

| | | | |
|-----------|---------------|--------------------------|------------------|
| | | 1.5 | Weber B (2015) |
| | | 5.38-288.23 (mean=57.06) | Wu et al. (2022) |
| 17 | water | -- | -- |
| 18 | Wooded tundra | -- | -- |
| 19 | Mixed tundra | -- | -- |
| 20 | Barren Tundra | -- | -- |

84 **Table S5.** Description of model simulation experiments.

| Simulation | Soil emissions | | Anthropogenic emissions |
|----------------------------------|----------------------------|------------------|--------------------------------|
| | Soil NO_x | Soil HONO | NO_x |
| Default | 1(MEGAN) | 0 | 1 |
| Base | 1(BDISNP) | 1 | 1 |
| NoSoilNr | 0 | 0 | 1 |
| NoSHONO | 1 | 0 | 1 |
| NoSNO_x | 0 | 1 | 1 |
| Base_redANO_x | 1 | 1 | 0.8/0.6/0.4/0.2/0 ^a |
| NoSoil_redANO_x | 0 | 0 | 0.8/0.6/0.4/0.2/0 ^b |

85 ^{a, b} The values represent the reduction ratios applied to the anthropogenic NO_x emissions in the
86 sensitivity simulations compared to the Base.

87

88 **Table S6.** Contribution of soil NO_x and HONO emissions to monthly average surface
 89 concentrations of NO₂ and HONO (unit: %).

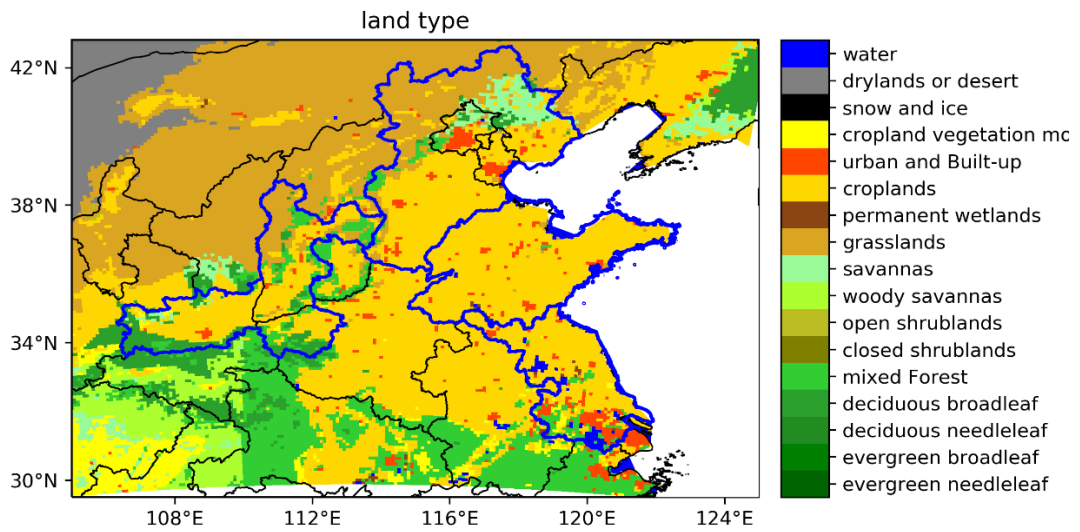
| Contribution | Surface NO ₂ concentrations | | | Surface HONO concentrations | | |
|------------------|--|------------|------------|-----------------------------|------------|------------|
| | Study region (CL) | BTH(CL) | FWP(CL) | Study region (CL) | BTH(CL) | FWP(CL) |
| SNO _x | 30.3(33.2) | 37.1(39.5) | 31.8(38.6) | 6.2(5.7) | 7.8(7.6) | 4.95(4.2) |
| SHONO | 3.1(2.3) | 1.8(1.75) | 2.7(3.1) | 35.6 (38.7) | 36.7(38.6) | 38.0(42.7) |
| Soil Nr | 32.7(34.7) | 38.4(40.5) | 33.9(41.3) | 38.2(20.0) | 40.3(42.0) | 40.1(44.6) |

90

91 **Table S7.** Effect of soil NO_x and HONO emissions on monthly average surface
 92 concentrations of MDA8 O₃, max-1h OH, and nitrate in BTH and FWP region during
 93 July 2018 (unit: %).

| Change | MDA8 O ₃ | | | max-1h ·OH | | | nitrate | | |
|----------------------|----------------------|----------------|----------------|----------------------|------------------|------------------|----------------------|----------------|----------------|
| | Study region (CL) | BTH (CL) | FWP (CL) | Study region (CL) | BTH (CL) | FWP (CL) | Study region (CL) | BTH (CL) | FWP (CL) |
| Soil NO _x | 15.3 (17.4) | 13.9 (15.0) | 14.6 (15.6) | -31.3 (-21.6) | -28.4 (-13.5) | -38.6 (-24.8) | 17.8 (22.4) | 29.6 (41.3) | 27.6 (32.8) |
| | 3.3 (3.0) | 3.5 (3.8) | 2.8 (3.1) | 10.0 (13.4) | 9.3 (13.1) | 10.3 (17.5) | 10.4 (11.3) | 10.9 (14.2) | 13.5 (15.2) |
| Soil HONO | 18.2 (20.0) | 16.9 (18.1) | 17.2 (18.6) | -24.3 (-12.5) | -22.6 (-4.4) | -32.2 (-13.6) | 31.8 (35.8) | 42.4 (57.8) | 42.7 (49.9) |
| | | | | | | | | | |

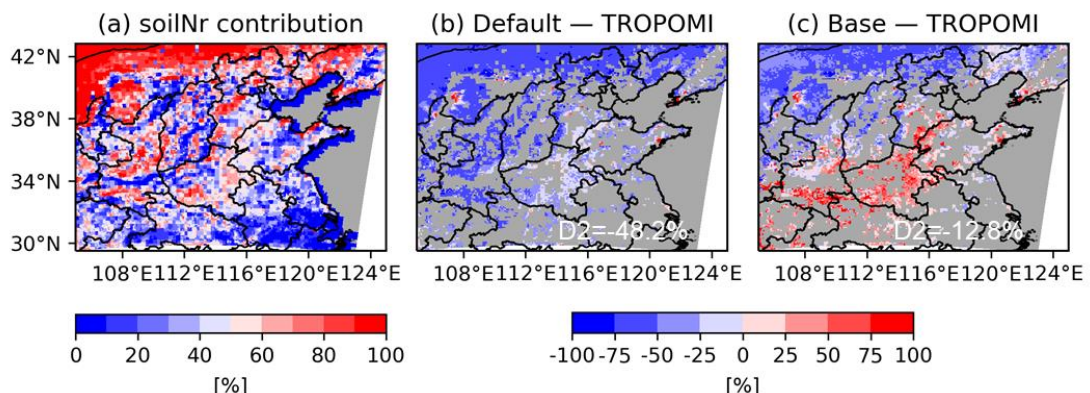
94



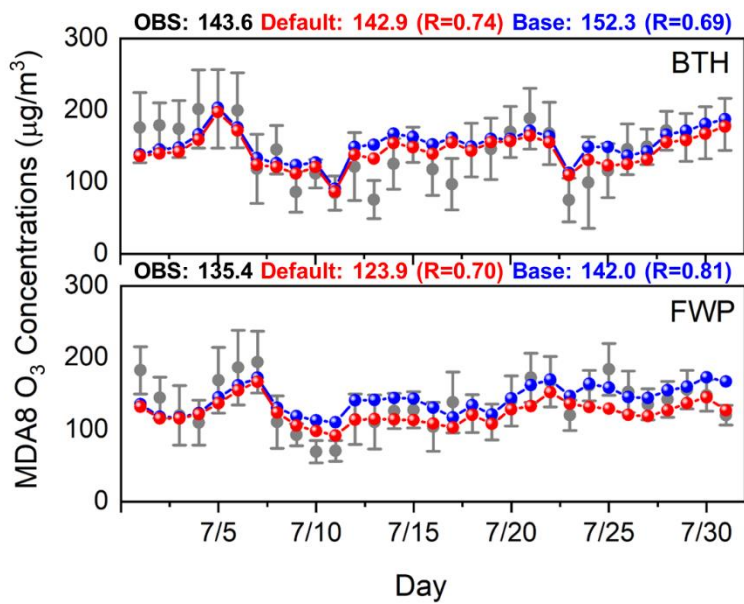
95

96 **Figure S1.** The land cover type over the simulation domain.

97



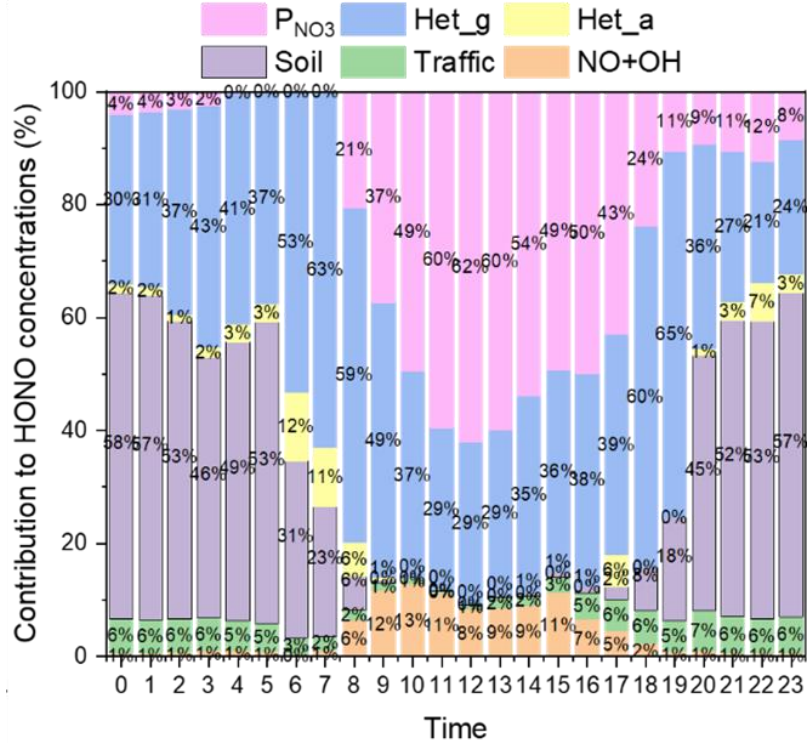
100 **Figure S2.** (a) Distribution of simulated contribution of soil Nr emissions to total Nr
 101 emissions, which includes the sources from anthropogenic emissions, soil emissions,
 102 and biomass burning. The difference of monthly mean tropospheric NO₂ VCD from
 103 TROPOMI observations and simulations ((b) Default, (c) Base). Statistics in each panel
 104 are the mean value averaged over the study region.
 105



106

107 **Figure S3.** Time series of observed (grey circles with bars representing the standard
 108 deviations) and simulated (Default in red and Base in blue) surface MDA8 O₃
 109 concentrations in the BTH and FWP regions, with the mean value and temporal
 110 correlation coefficients (R) shown in the upper corner.

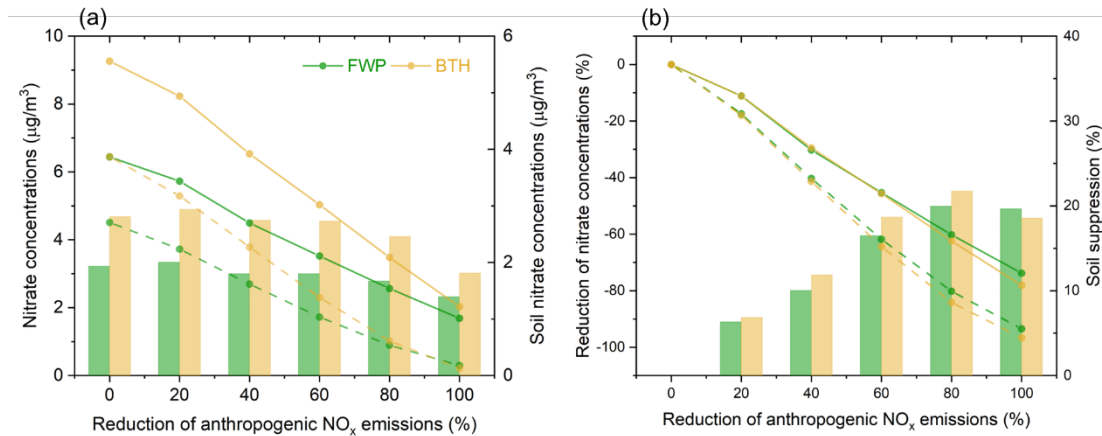
111



112

113 **Figure S4.** Average diurnal variations of contributions of different HONO sources to
 114 the simulated surface HONO at a rural station in Nanjing during July 2018. (P_{NO3},
 115 Het_g, Het_a, Soil, Traffic, and NO+OH represent HONO sources from the inorganic
 116 nitrate photolysis in the atmosphere, NO₂ heterogeneous reactions on ground and
 117 aerosol surfaces, soil emissions, traffic emissions, and the gas-phase formation,
 118 respectively).

119



122 **Figure S5.** The responses of nitrate concentrations to the reductions of anthropogenic
123 NO_x emissions (20%, 40%, 60%, 80% and 100%) relative to July 2018 levels in the
124 presence (solid line) and absence (dotted line) of soil nitrogen emissions. (The lines in
125 panel (a-b) are the nitrate concentrations and the relative reductions in nitrate
126 concentrations under different anthropogenic NO_x emission reductions, respectively.
127 The bars (right y-axis) in panel (a) show the corresponding nitrate contribution from
128 soil Nr emissions (denoted as soil nitrate concentrations) under different anthropogenic
129 NO_x emission reductions, which are determined as the difference between the solid and
130 dotted lines. The bars (right y-axis) in panel (b) show the suppression of nitrate
131 reduction due to the existence of soil nitrogen emissions (denoted as soil suppression),
132 which are determined as the difference between the solid and dotted lines. Green lines
133 and bars are the results in the FWP region, and the yellow are the results in the BTH
134 region.)

136 **Reference**

- 137 Finlayson-Pitts, B. J., Wingen, L. M., Sumner, A. L., Syomin, D., and Ramazan, K. A.:
138 The heterogeneous hydrolysis of NO₂ in laboratory systems and in outdoor and
139 indoor atmospheres: An integrated mechanism, *Phys. Chem. Chem. Phys.*, 5, 223-
140 242, 10.1039/b208564j, 2003.
- 141 Fu, X., Wang, T., Zhang, L., Li, Q., Wang, Z., Xia, M., Yun, H., Wang, W., Yu, C., Yue,
142 D., Zhou, Y., Zheng, J., and Han, R.: The significant contribution of HONO to
143 secondary pollutants during a severe winter pollution event in southern China,
144 *Atmos. Chem. Phys.*, 19, 1-14, 10.5194/acp-19-1-2019, 2019.
- 145 Li, G., Lei, W., Zavala, M., Volkamer, R., Dusante, S., Stevens, P., and Molina, L. T.:
146 Impacts of HONO sources on the photochemistry in Mexico City during the
147 MCMA-2006/MILAGO Campaign, *Atmos. Chem. Phys.*, 10, 6551-6567,
148 10.5194/acp-10-6551-2010, 2010.
- 149 Meng, F., Qin, M., Fang, W., Duan, J., Tang, K., Zhang, H., Shao, D., Liao, Z., Feng,
150 Y., Huang, Y., Ni, T., Xie, P., Liu, J., and Liu, W.: Measurement of HONO flux
151 using the aerodynamic gradient method over an agricultural field in the Huaihe
152 River Basin, China, *J. Environ. Sci.*, 114, 297-307, 10.1016/j.jes.2021.09.005,
153 2022.
- 154 Oswald, R., Behrendt, T., Ermel, M., Wu, D., Su, H., Cheng, Y., Breuninger, C.,
155 Moravek, A., Mougin, E., Delon, C., Loubet, B., Pommerening-Röser, A., Sörgel,
156 M., Pöschl, U., Hoffmann, T., Andreae, M. O., Meixner, F. X., and Trebs, I.:
157 HONO Emissions from Soil Bacteria as a Major Source of Atmospheric Reactive
158 Nitrogen, *Science*, 341, 1233-1235, 10.1126/science.1242266, 2013.
- 159 Rappenglück, B., Lubertino, G., Alvarez, S., Golovko, J., Czader, B., and Ackermann,
160 L.: Radical precursors and related species from traffic as observed and modeled at
161 an urban highway junction, *J. Air Waste Manage. Assoc.*, 63, 1270-1286, 2013.
- 162 Saliba, N. A., Mochida, M., and Finlayson-Pitts, B. J.: Laboratory studies of sources of
163 HONO in polluted urban atmospheres, *Geophys. Res. Lett.*, 27, 3229-3232,
164 10.1029/2000gl011724, 2000.
- 165 Sarwar, G., Roselle, S. J., Mathur, R., Appel, W., Dennis, R. L., and Vogel, B.: A

- 166 comparison of CMAQ HONO predictions with observations from the Northeast
167 Oxidant and Particle Study, *Atmos. Environ.*, 42, 5760-5770,
168 10.1016/j.atmosenv.2007.12.065, 2008.
- 169 Tang, K., Qin, M., Fang, W., Duan, J., Meng, F., Ye, K., Zhang, H., Xie, P., Liu, J., Liu,
170 W., Feng, Y., Huang, Y., and Ni, T.: An automated dynamic chamber system for
171 exchange flux measurement of reactive nitrogen oxides (HONO and NO_x) in
172 farmland ecosystems of the Huaihe River Basin, China, *Sci. Total Environ.*, 745,
173 140867, 10.1016/j.scitotenv.2020.140867, 2020.
- 174 Twigg, M. M., House, E., Thomas, R., Whitehead, J., Phillips, G. J., Famulari, D.,
175 Fowler, D., Gallagher, M. W., Cape, J. N., Sutton, M. A., and Nemitz, E.:
176 Surface/atmosphere exchange and chemical interactions of reactive nitrogen
177 compounds above a manured grassland, *Agric. For. Meteorol.*, 151, 1488-1503,
178 10.1016/j.agrformet.2011.06.005, 2011.
- 179 Wang, Y., Fu, X., Wang, T., Ma, J., Gao, H., Wang, X., and Pu, W.: Large Contribution
180 of Nitrous Acid to Soil-Emitted Reactive Oxidized Nitrogen and Its Effect on Air
181 Quality, *Environ. Sci. Technol.*, 57, 3516-3526, 10.1021/acs.est.2c07793, 2023.
- 182 Weber B, W. D., Tamm A, et al. : Biological soil crusts accelerate the nitrogen cycle
183 through large NO and HONO emissions in drylands, *Proc. Natl. Acad. Sci. U.S.A.*,
184 112(50): 15384-15389., 2015.
- 185 Wu, D., Horn, M. A., Behrendt, T., Müller, S., Li, J., Cole, J. A., Xie, B., Ju, X., Li, G.,
186 Ermel, M., Oswald, R., Fröhlich-Nowoisky, J., Hoor, P., Hu, C., Liu, M., Andreae,
187 M. O., Pöschl, U., Cheng, Y., Su, H., Trebs, I., Weber, B., and Sörgel, M.: Soil
188 HONO emissions at high moisture content are driven by microbial nitrate
189 reduction to nitrite: tackling the HONO puzzle, *ISME J.*, 13, 1688-1699,
190 10.1038/s41396-019-0379-y, 2019.
- 191 Wu, D., Zhang, J., Wang, M., An, J., Wang, R., Haider, H., Xu-Ri, Huang, Y., Zhang,
192 Q., Zhou, F., Tian, H., Zhang, X., Deng, L., Pan, Y., Chen, X., Yu, Y., Hu, C., Wang,
193 R., Song, Y., Gao, Z., Wang, Y., Hou, L., and Liu, M.: Global and Regional Patterns
194 of Soil Nitrous Acid Emissions and Their Acceleration of Rural Photochemical
195 Reactions, *J. Geophys. Res.: Atmos.*, 127, 10.1029/2021jd036379, 2022.

- 196 Xue, C., Ye, C., Zhang, Y., Ma, Z., Liu, P., Zhang, C., Zhao, X., Liu, J., and Mu, Y.:
197 Development and application of a twin open-top chambers method to measure soil
198 HONO emission in the North China Plain, *Sci. Total Environ.*, 659, 621-631,
199 10.1016/j.scitotenv.2018.12.245, 2019.
- 200 Zhang, J., An, J., Qu, Y., Liu, X., and Chen, Y.: Impacts of potential HONO sources on
201 the concentrations of oxidants and secondary organic aerosols in the Beijing-
202 Tianjin-Hebei region of China, *Sci. Total Environ.*, 647, 836-852,
203 10.1016/j.scitotenv.2018.08.030, 2019.
- 204 Zhang, L., Wang, T., Zhang, Q., Zheng, J., Xu, Z., and Lv, M.: Potential sources of
205 nitrous acid (HONO) and their impacts on ozone: A WRF-Chem study in a
206 polluted subtropical region, *J. Geophys. Res.: Atmos.*, 121, 3645-3662,
207 10.1002/2015jd024468, 2016.
- 208 Zhou, X., Zhang, N., TerAvest, M., Tang, D., Hou, J., Bertman, S., Alaghmand, M.,
209 Shepson, P. B., Carroll, M. A., Griffith, S., Dusanter, S., and Stevens, P. S.: Nitric
210 acid photolysis on forest canopy surface as a source for tropospheric nitrous acid,
211 *Nat. Geosci.*, 4, 440-443, 10.1038/ngeo1164, 2011.
- 212